Research Article | Vol. 28, No. 12 / 8 June 2020 / Optics Express 18112
Optics EXPRESS

Scale dependent performance of metallic light-trapping transparent electrodes

MENGDI SUN[1] AND PIETER G. KIK[1,2,*]

[1] CREOL, The College of Optics and Photonics, University of Central Florida, Orlando, Florida 32816, USA
[2] Physics Department, University of Central Florida, Orlando, Florida 32816, USA
[*] kik@creol.ucf.edu

Abstract: The optical and electrical performance of light trapping metallic electrodes is investigated. Reflection losses from metallic contacts are shown to be dramatically reduced compared to standard metallic contacts by leveraging total internal reflection at the surface of an added dielectric cover layer. Triangular wire arrays are shown to exhibit increased performance with increasing size, whereas cylindrical wires continue to exhibit diffractive losses as their size is increased. These trends are successfully correlated with radiation patterns from individual metallic wires. Triangular metallic electrodes with a metal areal coverage of 25% are shown to enable a polarization-averaged transmittance of >90% across the wavelength range 0.46-1.1 μm for an electrode width of 2 μm, with a peak transmission of 97%, a degree of polarization of <0.2%, and a sheet resistance of 0.35 Ω/sq. A new figure of merit is introduced to evaluate the light trapping potential of surface-shaped electrodes.

1. Introduction

Transparent electrodes are widely used in optoelectronic devices, such as solar cells, high speed photodetectors, imaging arrays and displays [1–12]. In scientific and industrial applications, a transmittance above 90% and sheet resistance below 100 Ω/sq are often required [13,14]. Achieving these performance numbers is hindered by the intrinsic trade-off between optical and electrical performance, with conductors causing absorption and reflection losses. Conductive thin film transparent electrodes have the benefit of a short carrier collection path at the cost of providing relatively low conductivity and introducing optical absorption losses [15,16]. Sparse transparent metallic wire electrodes can provide high conductivity but suffer from shadowing losses, polarization dependence, as well as a relatively long carrier collection path depending on wire spacing [17–22]. To address these challenges, a variety of structures have been investigated, such as encapsulated metal gratings [20,23–25], metallic contacts with high aspect ratio [26–28], periodic structures with plasmon-enhanced transmission [11,29–33] and patterned electrodes with textured surfaces [34–41].

A different approach to achieve metallic light-trapping electrodes has been proposed [34]. In this design, metallic wires with an inclined surface are covered by a thin dielectric layer. Light incident on the wires is reflected toward angles greater than the critical angle of the cover layer, resulting in light trapping and recovery of the reflected light. The resulting near-complete elimination of shadowing losses by such light trapping structures suggests that it may be possible to design electrodes that combine the advantages of thin-film transparent electrodes (short carrier collection path, low reflection losses) and metallic wire electrodes (high conductivity, low absorption losses), provided that the light trapping approach remains efficient at small wire spacing. To investigate this possibility, here the size dependent performance of light-trapping metallic electrodes is studied.

#391351 https://doi.org/10.1364/OE.391351
Journal © 2020 Received 5 Mar 2020; revised 5 May 2020; accepted 6 May 2020; published 2 Jun 2020

Optics EXPRESS

2. Size-dependent directional reflection by metallic nanowire electrodes

In the following, two types of light-trapping electrodes are considered: triangular and cylindrical wire interdigitated electrodes. Figure 1(a) shows a conventional metallic electrode design. Light incident on the planar metallic wires is reflected, causing shadowing losses proportional to the metal areal coverage *f*. Figure 1(b) shows a light-trapping triangular metal wire electrode. In this case a large fraction of light incident on the metal wires is reflected to angles greater than the critical angle and transmitted into the substrate after total internal reflection, dramatically reducing shadowing losses. Embedded cylindrical electrodes as shown in Fig. 1(c) also reflect a substantial portion of the incident light toward large angles and are thus expected to offer similar light trapping benefits.

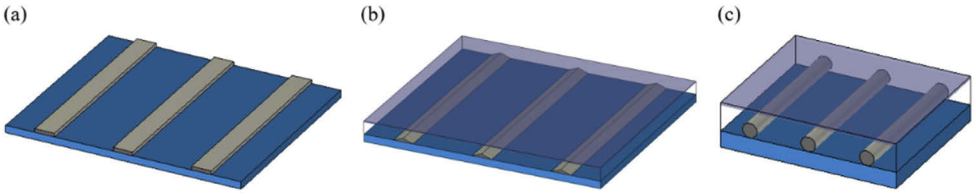

Fig. 1. Schematics of (a) a conventional planar metallic wire electrode, (b) a triangular light-trapping metal wire electrode and (c) a light-trapping cylindrical metal wire electrode.

In order to evaluate the size-dependent light trapping potential of the two different electrode geometries, we first perform numerical simulations of isolated triangular and cylindrical metallic wires embedded in a homogeneous dielectric environment. The structures are illuminated at normal incidence using a wavelength of 750 nm. Silver is used as the metal because of its relatively low optical-frequency losses and good electrical conductivity [42]. The refractive index of the surrounding medium was chosen to be n = 2, representative of the types of semiconductors used in solar-blind detectors [43], an application where reflection by metallic contacts introduces particularly significant optical losses. Note that similar light trapping could be achieved with the commonly employed glass-covered ethyl vinyl acetate (EVA) encapsulation material in silicon photovoltaic devices. Full-field electromagnetic simulations were carried out using the frequency domain finite element solver as implemented in CST Studio [44].

Figure 2(a) shows the simulated angular irradiance distribution of light reflected by isolated triangular silver wires with a fixed surface angle of 20° for four different widths: 200 nm, 600 nm, 1.2 μm and 2 μm. Results are shown for both TE polarization (top panel, electric field along the metal wire axis) and TM polarization (bottom panel, electric field normal to the wire axis). The results have been scaled by the total power incident on the metal wire to facilitate comparison between wires with different width.

Several key trends are observed. For small wire sizes, the angular distribution of the reflected light is relatively isotropic, resembling the omnidirectional radiation pattern of a line dipole. As the wire dimensions increase, the reflection becomes more directional, with reflection occurring predominantly toward angles close to 40° corresponding to the angle of specular reflection by the tilted electrode top surface. The observed angular narrowing indicates an increased light trapping potential. For example, at the chosen index of n = 2 any light reflected at angles larger than 30° can be trapped using total internal reflection at a planar top surface, whereas the fraction of light reflected toward smaller angles [the gray shaded region in Fig. 2(a)] would largely leak out of the structure. The angular distributions in Fig. 2(a) thus predict that the light trapping performance of triangular electrodes will gradually improve as the wire width approaches 1 μm, at which point shadowing losses may be largely mitigated. Note that off-normal illumination would modify the angular distributions, which in turn will affect the light trapping performance. A detailed study of such effects is currently underway. Figure 2(b) shows the corresponding results for

Optics EXPRESS

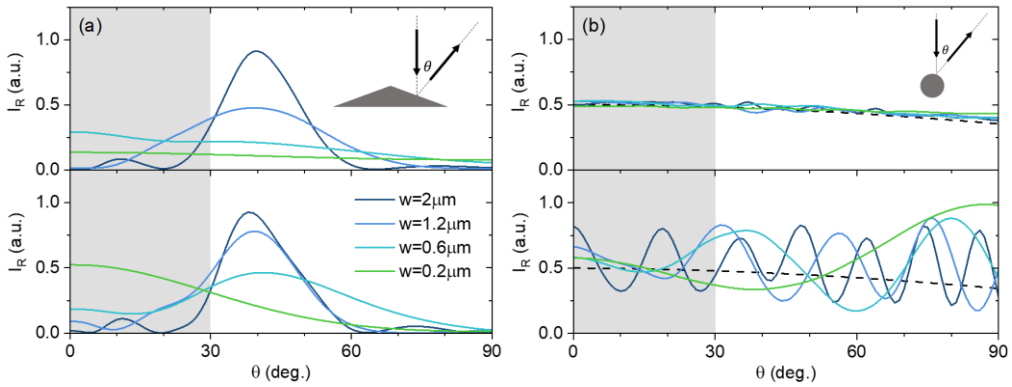

Fig. 2. Angle dependent reflected irradiance of (a) triangular and (b) cylindrical silver wires under TE (top panels) and TM (lower panels) illumination at λ_0=750 nm for different widths *w*. The dashed lines in (b) represent the angular distributions for macroscopic silver cylinders.

cylindrical silver wires. In contrast with the case for triangular wires, for TE illumination the angular distribution of the reflected light remains nearly isotropic for all electrode widths. For TM polarization, markedly different distributions are observed, with periodic angular patterns for all wire sizes, displaying more maxima as the wire diameter increases. These maxima result from the excitation of multipolar surface plasmon polariton (SPP) modes on the cylindrical wires, resulting in multipolar scattering patterns [45]. Note that for all cylindrical wire diameters, a significant fraction of the light is reflected toward small angle, suggesting that cylindrical wires are less suitable for optical trapping than triangular wires. At macroscopic scales, the angular distribution of reflected light under TE and TM illumination converges to a broad range of angles due to the curved nature of the reflecting surface, represented by the dashed lines in Fig. 2(b).

3. Size dependent light-trapping by metal nanowire arrays

To evaluate the performance of interdigitated light-trapping electrodes, periodic wire arrays were simulated. A large metal areal coverage of $f = 0.25$ was chosen for all structures, and the substrate and cover layer refractive index are assumed to be n = 2. A 133 nm thick anti-reflective coating with an index n = 1.41 is present on the cover layer, which minimizes surface reflection for the chosen reference wavelength of 750 nm.

Figure 3(a) shows the simulated transmitted (T), reflected (R), and absorbed (A) power fraction of a triangular wire interdigitated light trapping electrode as a function of wire width, averaged over TE and TM polarization. For all electrode widths the transmitted fraction significantly exceeds the 75% ray optics transmission limit (horizontal black dashed line) of traditional flat electrode arrays at the simulated 25% metal coverage. Absorption loss by the metallic wires accounts for <1.5 percent of the incident power for all electrode sizes studied.

The corresponding degree of polarization (DOP) of the transmitted light, defined here as $(T_{TE} - T_{TM}) / (T_{TE} + T_{TM})$ with T_{TE} and T_{TM} the transmitted TE and TM power fractions respectively, is shown in the lower panel. All structures exhibit a DOP magnitude below 10%, with the DOP decreasing as the electrode width increases. The corresponding effective sheet resistance for all widths is shown on the top axis. For large triangular electrodes (width w = 2 μm), high optical transmittance (>97%) and extremely low sheet resistance (<0.35 Ω/sq.) are achieved simultaneously. In the limit of larger ($\lambda >> \lambda_0$) electrodes, the optical performance will be affected solely by the reflection loss on the metal surfaces. Using the same literature values

Optics EXPRESS

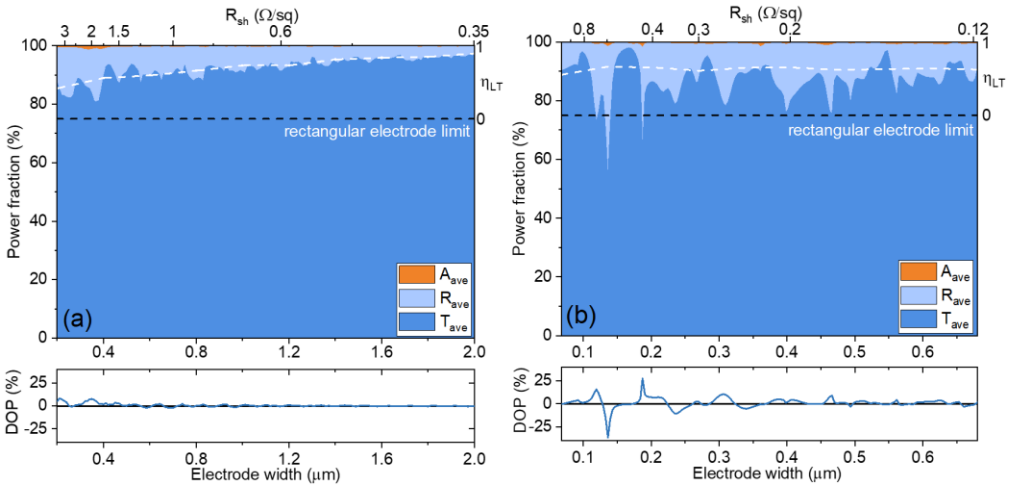

Fig. 3. Size-dependent absorption, reflection, transmission, light-trapping efficiency η_{LT}, and sheet resistance of (a) triangular and (b) cylindrical wire arrays at 25% areal metal coverage under normal-incidence unpolarized illumination at 750 nm light (top panels) and the corresponding degree of polarization of the transmitted light (lower panels). The white dashed line represents the predicted transmission based on single-wire radiation patterns.

for the Ag dielectric response, we arrive at a transmission of T = 99.88% for unpolarized incident light at λ_0 = 750 nm.

To quantify the light-trapping performance of the interdigitated electrode designs, we define the *light trapping efficiency* η_{LT} as the transmitted power fraction in excess of the flat electrode transmission limit, divided by the power fraction directly incident on the metal electrode lines, leading to the expression η_{LT}=1-(1-T)/*f*. This quantity is shown on the right axes in Fig. 3, where the top of the transmission curve represents the quantity η_{LT}. The light trapping efficiency is seen to increase gradually from 35% to 80% as the electrode width increases from 200 nm to 2 μm. The overall trend in the transmission and light trapping efficiency can be understood by considering the angular distributions from Fig. 2(a). For small electrode widths, a large fraction of the reflected light appears at angles smaller than the critical angle, resulting in incomplete light trapping. As the electrode width increases, the reflection becomes more directional and appears predominantly at angles beyond the critical angle (30°), resulting in increased light trapping. To verify this assertion quantitatively, the white dashed line in Fig. 3(a) shows the predicted size-dependent transmission based on the isolated-wire angular distributions in Fig. 2, neglecting multiple internal reflections. The resulting curve follows the overall transmission trend remarkably well, suggesting that at this moderate metal coverage (25%) effects related to multiple reflections do not dominate the optical performance.

Figure 3(b) shows the corresponding results for cylindrical wire interdigitated light trapping electrodes. In contrast to the results in Fig. 3(a), cylindrical wires do not produce a gradual increase in transmittance as the wire diameter is increased, and sharp transmission reductions are observed for specific wire sizes. The lack of a rising trend in transmission is attributed to the relatively isotropic reflection distributions shown in Fig. 2(b), causing an approximately constant reflection loss for all sizes. This is supported by the relatively constant predicted transmission (white dashed line) based on single-wire angular reflection distributions like those shown in Fig. 2(b). The isolated wire predictions do not reproduce the observed sharp transmission minima, suggesting that these are instead related to effects involving multiple adjacent wires, e.g. grating

Optics EXPRESS

resonances. The fact that such effects are relatively prominent in the case of cylindrical wires is also attributed to the more isotropic reflection patterns of cylindrical wires, which result in more power being radiated in the direction of adjacent wires. Note that absorption losses exceed those observed for triangular electrodes, attributed in large part to the grating-enhanced interaction of light with the lossy metallic wires. The corresponding DOP values in Fig. 3(b) show clear peaks and dips, indicating the polarization-dependent nature of the observed grating resonances.

To further clarify the origin of the features observed in Fig. 3, representative electromagnetic field distributions for periodic wire arrays with different electrode widths are shown in Fig. 4. Figure 4(a) shows the electric field magnitude distribution for a triangular wire array with the largest simulated width of 2 μm under TE illumination at 750 nm corresponding to T_{TE}=96.8%, with red regions indicating large field magnitude. Fringes are observed due to the interference of the incident wave with the reflected light from the electrode, both before and after internal reflection at the cover layer surface. The narrow fringes parallel to the inclined electrode surface result from upward reflection by the metal surface. The fringes above the dielectric cover layer indicate a small degree of reflection loss. The wider fringes to the side of the metallic electrode are indicative of interference of the directly transmitted incident wave and the downward propagating recovered light that has interacted with the metallic wire. Figure 4(b) shows the results for triangular wires with a four times smaller width of 500 nm, shown on the same size scale, with T_{TE}=89.6%. The larger contrast in the fringes above the structure is the result of the larger reflection losses caused by the less-directional reflection from the small wires. Figure 4(c) shows a special case of TM-polarized light incident on a 370 nm wide triangular wire array, corresponding to the deepest transmission dip in Fig. 3(a) with T_{TM}=74%. This electrode width is close to the silver SPP wavelength at the chosen 750 nm free-space wavelength. The transmission dip is attributed to the excitation of a standing SPP wave by the edges of the silver wire, resulting in resonantly enhanced dissipation and radiation losses. The resulting enhanced shadowing is clearly visible as the green-yellow region beneath the wires.

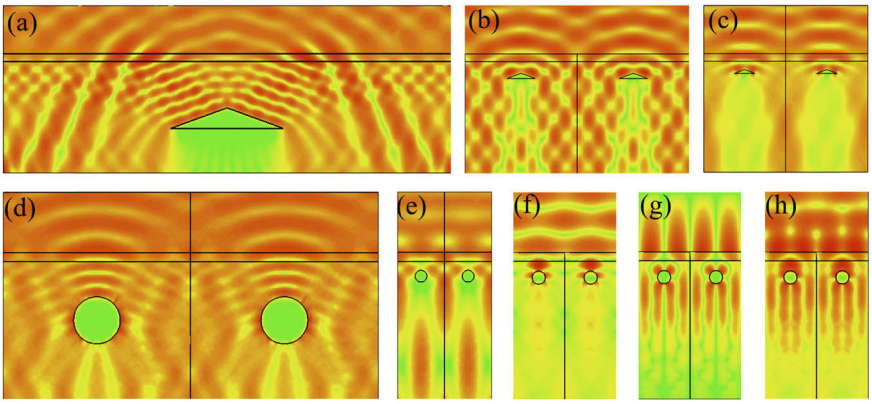

Fig. 4. Average electromagnetic field magnitude distribution of triangular wire arrays with (a) w = 2μm and (b) w = 500 nm under TE illumination, (c) w = 370 nm under TM illumination, and cylindrical wire arrays with (d) w = 680 nm under TM illumination, (e) w = 170 nm under TE illumination, and (f)-(h) w = 187.2 nm under TM illumination (E_x, E_z, and |E| contributions).

Figure 4(d) shows the field magnitude results for TM illumination of a cylindrical wire based light trapping electrode with wire width w = 680 nm with T_{TM}=88%. The curved standing waves in the cover layer are indicative of a relatively isotropic reflection distribution that results in incomplete light trapping. In addition, a relatively large field intensity is observed along the metal wire circumference due to the excitation of a multipolar SPP mode. Figure 4(e) shows the

Optics EXPRESS

results for a four times smaller diameter of w = 170 nm under TE illumination, coincidentally corresponding to a large transmission of T_{TE}=97.2%. Note that at this size the electrode spacing is less than the free-space wavelength, preventing any high angle reflection losses under normal incidence illumination. Finally, a very sharp T_{TM} dip is observed at w = 187.2 nm. To investigate the origin of this feature, panels in Figs. 4(f)–4(h) show the corresponding |E|, $|E_x|$ and $|E_z|$ distributions. Notably, the spatial period of this structure is just 0.3% below the free-space wavelength, allowing for standing waves that are weakly confined near the surface region. Inspection of the field distributions reveals a quadrupolar SPP mode on the cylindrical wires, coupled to a standing wave along the surface, similar to the process leading to Wood's anomalies. Such sharp grating resonances are suppressed in triangular wire arrays due to the more directional reflection from triangular wires.

4. Spectral performance

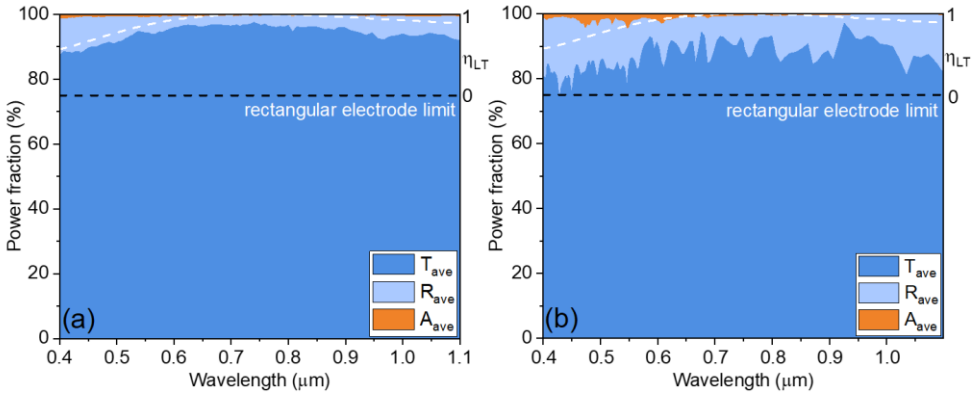

Fig. 5. Spectral dependence of the absorption, reflection, transmission, and light-trapping efficiency η_{LT} of (a) triangular and (b) cylindrical wire arrays at 25% areal metal coverage under normal-incidence unpolarized illumination. The white dashed line represents the transmission spectrum of the AR coating in the absence of metal wires.

The results shown thus far were achieved under fixed wavelength excitation. For optoelectronic devices such as solar cells and photodetectors, the spectral response is of critical importance. Figure 5 shows the spectral response of 2 μm wide triangular electrodes and 0.68 μm wide cylindrical electrodes both at f = 0.25 for normally incident unpolarized light in the range 0.4 – 1.1 μm. The triangular wire array exhibits high transmittance (T > 86%) across the entire spectrum, with T > 93% from 550-900 nm. At all wavelengths, the predominant contribution to transmission loss is reflection, with absorption losses making up only a small fraction of the total losses. A gradual spectral variation of the transmission is observed, which is attributed to the presence of the AR coating, which was optimized for 750 nm light. This is confirmed by the similar spectral shape of the transmission of the AR coating in the absence of metal wires (white dashed line). Figure 5(b) shows the corresponding results for the cylindrical wire light-trapping electrode. In this case, a large number of sharp transmission dips is seen, attributed to grating effects. As argued above, the prevalence of grating resonances is due to the more isotropic radiation patterns from cylindrical wires, which increases the possibility of multiple reflections on adjacent wires. Note that similar grating effects were also observed in work on mesoscale wire arrays investigated by Saive *et al* [27]. In addition to the grating-enhanced reflection losses, increased absorption due to SPP resonances is also observed at small wavelengths. As a result, the overall light-trapping performance of triangular electrodes typically exceeds that of cylindrical

Optics EXPRESS

electrodes, providing higher transmission, reduced polarization dependence, and lower spectral variation.

5. Figure of merit

The light trapping designs discussed above call for a new Figure of Merit (FOM) in order to compare different electrode geometries, as argued below. The performance of transparent electrodes is commonly evaluated in terms of a figure of merit (FOM) expressed as the ratio of the electrical sheet conductivity σ_s to any introduced optical loss processes [19,46–49]. For transparent conductive films where absorption is the main source of optical loss, the FOM typically takes the form $\zeta = \sigma_s/\alpha$. In systems where shadowing contributes significantly to the optical losses, a convenient form is $\zeta=\sigma_s/(1\text{-}T)$ where the denominator now includes all optical losses including those from shadowing, and where the sheet conductivity is an effective value that takes into account the spatial distribution of the metal. However, since the effective sheet conductivity of the light trapping systems discussed above can be increased almost arbitrarily by placing more metal directly under the wires ("in the shadow"), we propose the following light-trapping FOM to compare the performance potential of different wire shapes:

$$\zeta_{LT} = \frac{f}{1-T} \tag{1}$$

This FOM captures the fact that transmission loss (factor 1-T in the denominator) is a disadvantage, whereas large metal areal coverage (f) is an advantage, allowing tall conductive structures to be placed on the substrate. Note that this FOM does not include statements about the exact total electrode height, but only considers the *opportunity* of placing tall electrodes in a fraction f of the surface. The appropriateness of this choice will be demonstrated below.

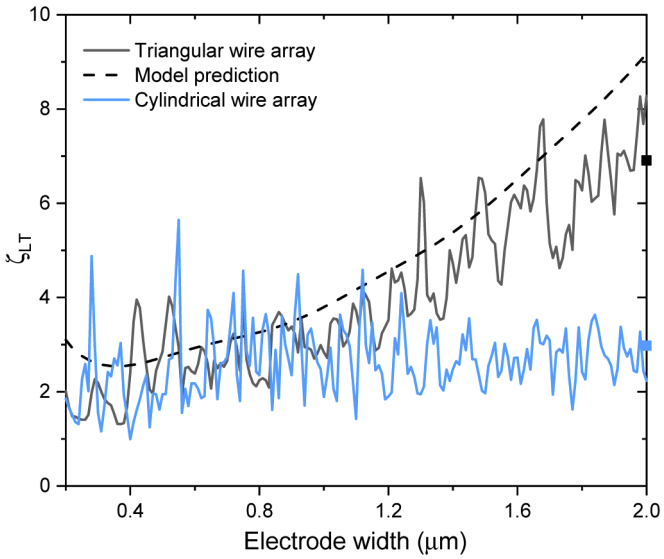

Fig. 6. Light-trapping figure of merit ζ_{LT} of triangular (black curve) and cylindrical (blue curve) wire arrays. The black dashed line represents a model prediction based on isolated triangular wire angular reflection distributions.

Figure 6 shows the introduced light-trapping figure of merit of different electrode geometries at an incident wavelength of 750 nm. The light-trapping FOM of cylindrical electrodes (blue line) is seen to be relatively unchanged as the size is increased, because of the aforementioned

Optics EXPRESS

broad angular distribution of the reflected light from cylindrical electrodes for all electrode sizes. In contrast, the light-trapping FOM of triangular electrodes gradually improves for increasing size due to the increase in directionality of the reflected light, enabling increasingly improved transmission. For comparison, the dashed line represents the predicted light-trapping FOM based on the radiation pattern of isolated triangular electrodes, taking into account analytical expressions for the angle-dependent reflection at the top surface of the structure. This simplified model reproduces the overall trend and absolute value of the ζ_{LT}. Finally, to demonstrate that the chosen form of FOM fairly evaluates the suitability of the electrode geometry for light trapping independent of the height of the wires, we calculated ζ_{LT} for an array of 2 μm wide triangular electrodes with a 1.4 μm tall rectangular base and 2 μm wide hemicylindrical electrodes with a 1.4 μm tall rectangular base using the same numerical approach as above. The corresponding result are indicated by the square symbols in Fig. 6. Despite the fact that this structure has an 8.6 times larger sheet conductivity, the obtained ζ_{LT} values are indeed very close to those of the triangular and cylindrical wires of the same width. This confirms that our choice of light-trapping FOM is a good measure of the light trapping efficiency of a particular electrode surface shape, while largely removing the dependence of wire height or aspect ratio.

6. Summary

In conclusion, we have studied the size-dependent optical and electrical performance of triangular and cylindrical metallic wire grid light-trapping transparent electrodes. A gradual increase in optical performance of triangular wire electrodes was observed as the wire width increased. This trend was successfully explained in terms of the size-dependent angular distribution of the reflection from individual wires. Cylindrical nanowires showed no such size dependent trend, matching model predictions based on individual wire reflection distributions. The spectral response of triangular wire arrays was found to be broadband and relatively smooth, whereas cylindrical nanowire arrays support multiple grating resonances leading to large spectral variation in transmission and a large degree of polarization of the transmitted light. All observations indicate that micron-sized triangular wire light trapping transparent electrodes substantially outperform cylindrical nanowire light trapping electrodes in terms of absolute transmission, spectral dependence, and polarization insensitivity. Triangular electrodes with a width of 2 μm and a metal coverage of 25% were found to recover as much as 88% of the unpolarized light incident on the metal portion of the wire array, resulting in 97% optical transparency and 0.35 Ω/sq. sheet resistance at a wavelength of 750 nm, with a broadband optical transmittance exceeding 86% in the wavelength range 400 nm-1.1 μm. A new figure of merit was introduced that evaluates the overall light trapping potential of transparent electrodes based on embedded shaped metallic wire arrays.

Funding

National Science Foundation (ECCS-1650002).

Disclosures

The authors declare no conflicts of interest.

References

1. T. Sannicolo, M. Lagrange, A. Cabos, C. Celle, J. P. Simonato, and D. Bellet, "Metallic Nanowire-Based Transparent Electrodes for Next Generation Flexible Devices: a Review," Small **12**(44), 6052–6075 (2016).
2. Z. Liu, J. Xu, D. Chen, and G. Shen, "Flexible electronics based on inorganic nanowires," Chem. Soc. Rev. **44**(1), 161–192 (2015).
3. P. Kou, L. Yang, C. Chang, and S. He, "Improved Flexible Transparent Conductive Electrodes based on Silver Nanowire Networks by a Simple Sunlight Illumination Approach," Sci. Rep. **7**(1), 42052 (2017).

Optics EXPRESS

4. K. Ellmer, "Past achievements and future challenges in the development of optically transparent electrodes," Nat. Photonics **6**(12), 809–817 (2012).
5. S. J. Kim, J.-H. Kang, M. Mutlu, J. Park, W. Park, K. E. Goodson, R. Sinclair, S. Fan, P. G. Kik, and M. L. Brongersma, "Anti-Hermitian photodetector facilitating efficient subwavelength photon sorting," Nat. Commun. **9**(1), 316 (2018).
6. E. C. Garnett, W. Cai, J. J. Cha, F. Mahmood, S. T. Connor, M. Greyson Christoforo, Y. Cui, M. D. McGehee, and M. L. Brongersma, "Self-limited plasmonic welding of silver nanowire junctions," Nat. Mater. **11**(3), 241–249 (2012).
7. V. E. Ferry, J. N. Munday, and H. A. Atwater, "Design Considerations for Plasmonic Photovoltaics," Adv. Mater. **22**(43), 4794–4808 (2010).
8. J. van de Groep, P. Spinelli, and A. Polman, "Transparent Conducting Silver Nanowire Networks," Nano Lett. **12**(6), 3138–3144 (2012).
9. V. E. Ferry, L. A. Sweatlock, D. Pacifici, and H. A. Atwater, "Plasmonic Nanostructure Design for Efficient Light Coupling into Solar Cells," Nano Lett. **8**(12), 4391–4397 (2008).
10. L. Hu, H. S. Kim, J.-Y. Lee, P. Peumans, and Y. Cui, "Scalable Coating and Properties of Transparent, Flexible, Silver Nanowire Electrodes," ACS Nano **4**(5), 2955–2963 (2010).
11. H. A. Atwater and A. Polman, "Plasmonics for improved photovoltaic devices," Nat. Mater. **9**(3), 205–213 (2010).
12. V. E. Ferry, M. A. Verschuuren, H. B. T. Li, E. Verhagen, R. J. Walters, R. E. I. Schropp, H. A. Atwater, and A. Polman, "Light trapping in ultrathin plasmonic solar cells," Opt. Express **18**(S2), A237–A245 (2010).
13. H. C. Chu, Y. C. Chang, Y. Lin, S. H. Chang, W. C. Chang, G. A. Li, and H. Y. Tuan, "Spray-Deposited Large-Area Copper Nanowire Transparent Conductive Electrodes and Their Uses for Touch Screen Applications," ACS Appl. Mater. Interfaces **8**(20), 13009–13017 (2016).
14. R. Zhang and M. Engholm, "Recent Progress on the Fabrication and Properties of Silver Nanowire-Based Transparent Electrodes," Nanomaterials **8**(8), 628 (2018).
15. X. Wang, L. Zhi, and K. Müllen, "Transparent, Conductive Graphene Electrodes for Dye-Sensitized Solar Cells," Nano Lett. **8**(1), 323–327 (2008).
16. Z. Wu, "Transparent, Conductive Carbon Nanotube Films," Science **305**(5688), 1273–1276 (2004).
17. H. Lu, X. Ren, D. Ouyang, and W. C. H. Choy, "Emerging Novel Metal Electrodes for Photovoltaic Applications," Small **14**(14), 1703140 (2018).
18. J.-Y. Lee, S. T. Connor, Y. Cui, and P. Peumans, "Solution-Processed Metal Nanowire Mesh Transparent Electrodes," Nano Lett. **8**(2), 689–692 (2008).
19. D. S. Ghosh, T. L. Chen, and V. Pruneri, "High figure-of-merit ultrathin metal transparent electrodes incorporating a conductive grid," Appl. Phys. Lett. **96**(4), 041109 (2010).
20. P. Kuang, J. M. Park, G. Liu, Z. Ye, W. Leung, S. Chaudhary, D. Lynch, K. M. Ho, and K. Constant, "Metal-nanowall grating transparent electrodes: achieving high optical transmittance at high incident angles with minimal diffraction," Opt. Express **21**(2), 2393–2401 (2013).
21. S. Ye, A. R. Rathmell, Z. Chen, I. E. Stewart, and B. J. Wiley, "Metal nanowire networks: the next generation of transparent conductors," Adv. Mater. **26**(39), 6670–6687 (2014).
22. S. De, T. M. Higgins, P. E. Lyons, E. M. Doherty, P. N. Nirmalraj, W. J. Blau, J. J. Boland, and J. N. Coleman, "Silver Nanowire Networks as Flexible, Transparent, Conducting Films: Extremely High DC to Optical Conductivity Ratios," ACS Nano **3**(7), 1767–1774 (2009).
23. A. W. Blakers, "Shading losses of solar-cell metal grids," J. Appl. Phys. **71**(10), 5237–5241 (1992).
24. F. H. Chen, S. Pathreeker, J. Kaur, and I. D. Hosein, "Increasing light capture in silicon solar cells with encapsulants incorporating air prisms to reduce metallic contact losses," Opt. Express **24**(22), A1419–A1430 (2016).
25. J. N. Munday and H. A. Atwater, "Large Integrated Absorption Enhancement in Plasmonic Solar Cells by Combining Metallic Gratings and Antireflection Coatings," Nano Lett. **11**(6), 2195–2201 (2011).
26. J. Lossen, D. Rudolph, L. J. Koduvelikulathu, R. Carvalho, M. P. Rossetto, O. Borsato, E. Bortoletto, and M. Galiazzo, "Double Printing nPERT Cells with Narrow Contact Layers," Energy Procedia **92**, 939–948 (2016).
27. R. Saive and H. A. Atwater, "Mesoscale trumps nanoscale: metallic mesoscale contact morphology for improved light trapping, optical absorption and grid conductance in silicon solar cells," Opt. Express **26**(6), A275–A282 (2018).
28. J. S. Ward, A. Duda, D. J. Friedman, J. Geisz, W. McMahon, and M. Young, "High aspect ratio electrodeposited Ni/Au contacts for GaAs-based III-V concentrator solar cells," Prog. Photovoltaics **23**(5), 646–653 (2015).
29. C. Genet and T. W. Ebbesen, "Light in tiny holes," Nature **445**(7123), 39–46 (2007).
30. S. J. Lee, Z. Ku, A. Barve, J. Montoya, W. Y. Jang, S. R. Brueck, M. Sundaram, A. Reisinger, S. Krishna, and S. K. Noh, "A monolithically integrated plasmonic infrared quantum dot camera," Nat. Commun. **2**(1), 286 (2011).
31. L. Martin-Moreno, F. J. Garcia-Vidal, H. J. Lezec, K. M. Pellerin, T. Thio, J. B. Pendry, and T. W. Ebbesen, "Theory of extraordinary optical transmission through subwavelength hole arrays," Phys. Rev. Lett. **86**(6), 1114–1117 (2001).
32. K. Aydin, V. E. Ferry, R. M. Briggs, and H. A. Atwater, "Broadband polarization-independent resonant light absorption using ultrathin plasmonic super absorbers," Nat. Commun. **2**(1), 517 (2011).
33. F. J. Beck, A. Polman, and K. R. Catchpole, "Tunable light trapping for solar cells using localized surface plasmons," J. Appl. Phys. **105**(11), 114310 (2009).
34. P. G. Kik, "Catoptric electrodes: transparent metal electrodes using shaped surfaces," Opt. Lett. **39**(17), 5114–5117 (2014).

Optics EXPRESS

35. R. Saive, M. Boccard, T. Saenz, S. Yalamanchili, C. R. Bukowsky, P. Jahelka, Z. J. Yu, J. Shi, Z. Holman, and H. A. Atwater, "Silicon heterojunction solar cells with effectively transparent front contacts," Sustainable Energy Fuels **1**(3), 593–598 (2017).
36. R. Saive, A. M. Borsuk, H. S. Emmer, C. R. Bukowsky, J. V. Lloyd, S. Yalamanchili, and H. A. Atwater, "Effectively Transparent Front Contacts for Optoelectronic Devices," Adv. Opt. Mater. **4**(10), 1470–1474 (2016).
37. S. Xie, Z. Ouyang, N. Stokes, B. Jia, and M. Gu, "Enhancing the optical transmittance by using circular silver nanowire networks," J. Appl. Phys. **115**(19), 193102 (2014).
38. Z. Zhao, K. X. Wang, and S. Fan, "Analysis of an anti-reflecting nanowire transparent electrode for solar cells," J. Appl. Phys. **121**(11), 113109 (2017).
39. T. Gao and P. W. Leu, "The role of propagating modes in silver nanowire arrays for transparent electrodes," Opt. Express **21**(S3), A419–A429 (2013).
40. P. B. Catrysse and S. Fan, "Nanopatterned Metallic Films for Use As Transparent Conductive Electrodes in Optoelectronic Devices," Nano Lett. **10**(8), 2944–2949 (2010).
41. I. Massiot, N. Vandamme, N. Bardou, C. Dupuis, A. Lemaître, J.-F. Guillemoles, and S. Collin, "Metal Nanogrid for Broadband Multiresonant Light-Harvesting in Ultrathin GaAs Layers," ACS Photonics **1**(9), 878–884 (2014).
42. P. B. Johnson and R. W. Christy, "Optical Constants of the Noble Metals," Phys. Rev. B **6**(12), 4370–4379 (1972).
43. J. F. Muth, J. D. Brown, M. A. L. Johnson, Z. Yu, R. M. Kolbas, J. W. Cook, and J. F. Schetzina, "Absorption Coefficient and Refractive Index of GaN, AlN and AlGaN Alloys," MRS Internet J. Nitride Semicond. Res. **4**(S1), 502–507 (1999).
44. CST Studio Suite, Dassault Systèmes Simulia, Providence, Rhode Island, 2017.
45. O. J. F. Martin, "Plasmon Resonances in Nanowires with a Non—regular Cross-Section," in *Optical Nanotechnologies: The Manipulation of Surface and Local Plasmons*, J. Tominaga and D. P. Tsai, eds. (Springer Berlin Heidelberg, 2003), pp. 183–210.
46. S. De, P. J. King, P. E. Lyons, U. Khan, and J. N. Coleman, "Size effects and the problem with percolation in nanostructured transparent conductors," ACS Nano **4**(12), 7064–7072 (2010).
47. R. G. Gordon, "Criteria for Choosing Transparent Conductors," MRS Bull. **25**(8), 52–57 (2000).
48. G. Haacke, "New figure of merit for transparent conductors," J. Appl. Phys. **47**(9), 4086–4089 (1976).
49. B. S. Shim, J. Zhu, E. Jan, K. Critchley, and N. A. Kotov, "Transparent conductors from layer-by-layer assembled SWNT films: importance of mechanical properties and a new figure of merit," ACS Nano **4**(7), 3725–3734 (2010).